Available online at www.sciencedirect.com

ScienceDirect

Ceramics International 40 (2014) 4383–4388

CERAMICS INTERNATIONAL

www.elsevier.com/locate/ceramint

Electrical characterization of ZnO-based thin film nanodiodes fabricated through atomic layer deposition: Effect of electron beam irradiation on interfacial property

Yil-Hwan You[a], Min-Kyeong Kim[a], Byeong-Cheol Lee[b], Jinha Hwang[a,*]

[a]*Department of Materials Science and Engineering, Hongik University, Seoul 121-791, Republic of Korea*
[b]*Korea Atomic Energy Research Institute, Daejeon 305-353, Republic of Korea*

Received 20 July 2013; received in revised form 23 August 2013; accepted 26 August 2013
Available online 6 September 2013

Abstract

ZnO thin films were deposited onto p-type (P-Si) Si wafers using atomic layer deposition. The rectifying performance of the deposited ZnO thin films was confirmed by current–voltage characteristics. P-Si/ZnO-based nanodiodes were subjected to electron irradiation. Depending on the irradiation conditions, the diode performance changed significantly. At 0.8 MeV, the diode was degraded in terms of both forward and reverse currents. At 2.5 MeV, the reverse current in the nanodiode decreased and the forward current increased, leading to significant enhancement in the current ratio. The electrical response was monitored using impedance spectroscopy. Impedance analysis indicated that depletion regions are significantly affected by electron irradiation.
© 2013 Elsevier Ltd and Techna Group S.r.l. All rights reserved.

Keywords: Atomic layer deposition; Nanodiodes; Impedance spectroscopy; Depletion region; Electron irradiation

1. Introduction

p-n junctions are critical circuit elements in electronic and optoelectronic devices. However, oxide-based nanodiodes have been limited because of the rarity of p-type conducting oxides [1–5]. There are no alternative materials equivalent to Si in which p- and n-type conduction can be easily realized through the use of alio-valent dopants, e.g., group III or V elements. Indeed, no semiconducting oxide has shown unambiguous evidence of both conduction types.

ZnO is a well-known semiconducting oxide used in a number of optoelectronic applications including transparent electrodes and channel materials. It has a wide bandgap of 3.3 eV that can be controlled to achieve a wide conduction range of 10^{-7}–$10^{2}\ \Omega^{-1}\cdot\text{cm}^{-1}$ through aliovalent doping [6,7]. ZnO can be integrated with other p-type conducting materials for rectifying diode performance [1–5]. Diode performance has not been extensively studied. Previous work has focused on the fabrication of p-n diodes and their applications [1–4,7]. Artificial control of p-n diode devices has not been attempted. The corresponding diode performance is closely related to the depletion regions that originate from contact between dissimilar materials. Electron irradiation has been gaining attention because it does not result in any physical damage or radioactive radiation. Except for e-beam testing in solid state devices, there have been a limited number of works focusing on solid state devices composed of functional thin films: MOS-transistors, graphene field effect transistors, carbon nanotube transistors, and light-emitting diodes were affected by electron beam radiation [8–11] in the form of irradiation defects, oxide charging, efficient activation in functional dopants, and silicon charging.

Recently, the current research group reported the induction of charge-trapping behavior in high-*k* materials [12]. This behavior can be utilized in nano-floating gate memories that can be used as next-generation nonvolatile memories.

The current research is based on the interaction of an electron beam with diode interfaces, which determines the diode performance. ZnO thin films were selected as a model system because they offer n-type conduction and a facile approach to form atomically uniform interfaces using atomic

*Corresponding author. Tel.: +82 2 320 3069; fax: +82 2 333 0127.
E-mail address: jhwang@wow.hongik.ac.kr (J. Hwang).

0272-8842/$ - see front matter © 2013 Elsevier Ltd and Techna Group S.r.l. All rights reserved.
http://dx.doi.org/10.1016/j.ceramint.2013.08.109

layer deposition (ALD). The ALD of ZnO is enabled using the well-known Zn precursor diethyl zinc (DEZ, $Zn(C_2H_5)_2$). Well-controlled ZnO thin films contribute to reproducible p-n junctions with p-Si wafers. This paper reports the fabrication and characterization of p-n diodes based on atomic layer deposition, and the artificial control of diode performance via highly energetic electron beam irradiation. In addition to the elementary characterization of thin films, electrical characterization was carried out via dc-based and ac-based techniques, i.e., current–voltage characteristics and impedance spectroscopy, respectively. Supplementary features of both approaches are combined for rectifying current–voltage characteristics in terms of the underlying mechanism and effective property control.

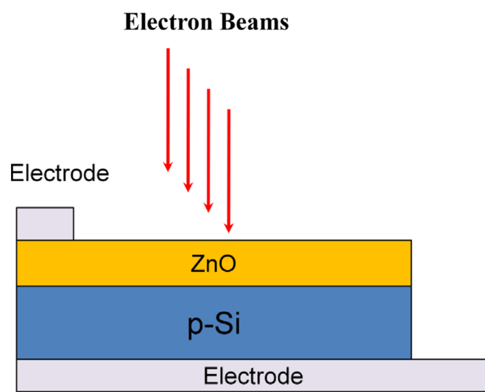

Fig. 1. Schematic of the nanodiodes based on a p-type Si wafer and an n-type ZnO thin film.

2. Experimental procedure

To fabricate oxide-based nanodiodes, ZnO thin films were deposited onto p-type Si wafers (resistivity of 1–20 Ω · cm and dopant concentration of 7×10^{14}–$1 \times 10^{16}/cm^3$) using ALD where DEZ and H_2O were employed as the sources of Zn and oxygen, respectively, at 140 °C. Excess DEZ and H_2O were removed by purging with Ar gas. The deposition rate was calculated to be approximately 1.4 Å per cycle. After the calculation of ALD cycles, ZnO thin films were deposited onto p-type Si wafers by controlling the film thickness to approximately 30 nm. Before film deposition, the Si wafers were cleaned using organic solvents and native oxides were removed using buffered oxide etchants.

The deposited ZnO thin films were subjected to physical and chemical characterization. Physical characterization involved X-ray diffraction for structural analysis, atomic force microscopy for surface morphology, and spectroscopic ellipsometry for thickness monitoring. Chemical characterization involved X-ray photoelectron spectroscopy (XPS). The films were subjected to electron beam irradiation using a commercial electron beam accelerator (EBTech. Co., Daejeon, Korea).

For electrical characterization, the deposited ZnO thin films were subjected to the thermal evaporation of Al electrodes (thickness of 1000 Å and diameter of 160 μm), which function as top electrodes in p-Si/ZnO diodes, as schematically shown in Fig. 1. The underlying Si wafers were wired using silver paste to guarantee ohmic contacts between the electrodes. A two-point electrode configuration was applied to dc-based current-voltage characteristics determination (Agilent 4156C,

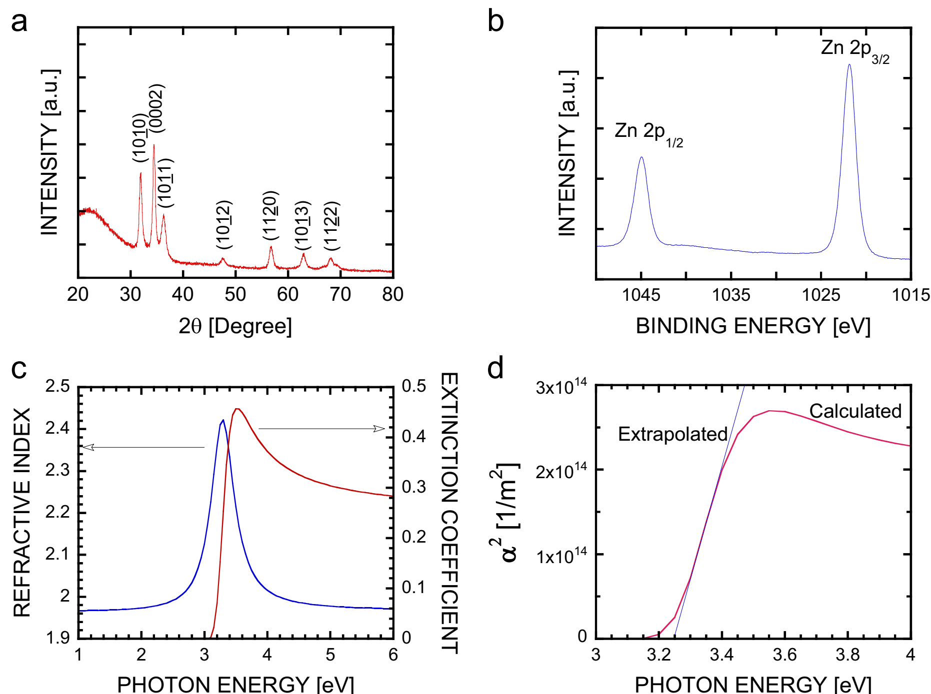

Fig. 2. Physical analyses of ZnO thin films deposited through atomic layer deposition: (a) X-ray diffraction, (b) Zn core spectrum obtained from XPS measurements, (c) calculated refractive index and extinction coefficient as a function of photon energy, and (d) squared absorption coefficient as a function of photon energy for the calculation of bandgap.

Semiconductor Parameter Analyzer, Palo Alto, CA, USA) and ac-based impedance spectroscopy (Solatron 1260, Frequency Response Analyzer, Hampshire, UK). The obtained impedance spectra were analyzed using the commercial software "ZVIEW" (Scrivner, London, UK).

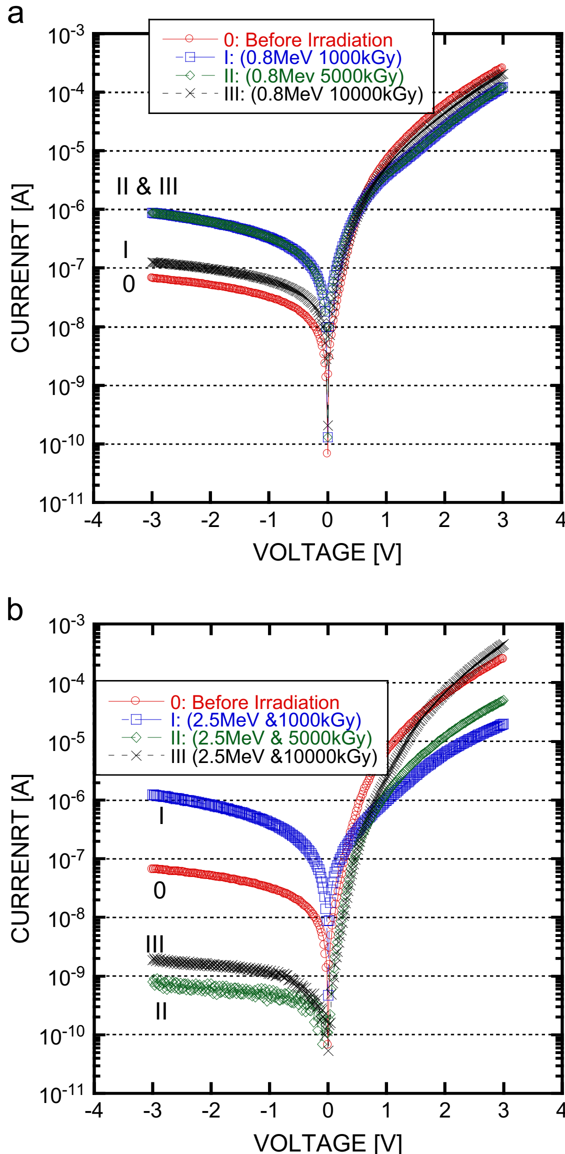

Fig. 3. Current–voltage characteristics of ZnO thin films as a function of electron dose: (a) 1000, 5000, 10,000 kGy at 0.8 MeV, and (b) 1000, 5000, 10,000 kGy at 2.5 MeV.

3. Results and discussion

The deposited ZnO thin films were characterized in terms of their physical and chemical properties. The physical characterization of ZnO included surface morphology, crystal structure, and bandgap measurements. The X-ray diffraction patterns of the thin films (Fig. 2(a)) showed distinct diffraction peaks, unlike amorphous structures whose patterns do not show any crystalline peaks or large degree of peak broadening. The crystalline features somewhat corroborate the larger values of surface roughness represented by their root-mean square (RMS) values, i.e, 0.796 nm. The X-ray photoelectron spectroscopy (XPS) analysis supports the formation of ZnO with Zn^{+2}, confirmed by Zn $2p_{3/2}$ and Zn $2p_{1/2}$ peaks as shown in Fig. 2(b). Spectroscopic ellipsometry was applied to obtain the optical constants, i.e., n (refractive index) and k (extinction coefficient). The resolved optical constants, i.e., n and k can be exploited in order to estimate the optical bandgap through the absorption coefficient including the wavelength-dependence of the extinction coefficient through the following equation [13],

$$\alpha(E) = \frac{4\pi k}{\lambda} \quad (1)$$

The semiconductors are classified into either direct and indirect bandgaps depending on the relative position in the wave-vector describing the minimum in the conduction and the maximum in the valence band. ZnO is known to be a direct bandgap semiconductor. In the direct bangap semiconductor, the corresponding absorption coefficient is defined by the following equation

$$\alpha(E) = A(E - E_g)^{1/2} \quad (2)$$

From the information of α^2 versus E (photon energy), the optical bandgap is estimated to be the intercept at $\alpha^2 = 0$. Based on Fig. 2(c) and Eqs. (1) and (2), the optical bandgap is extrapolated to be 3.24 eV. The fully characterized ZnO thin films were combined onto p-type Si wafers with a resistivity in the range 1–20 Ω·cm and a dopant concentration in the range 10^{15}–10^{16} per cm^3. The crystallinity of the ZnO thin films allows for high performance in terms of both forward and reverse currents (see Fig. 3 for an example).

ZnO-based nanodiodes were subjected to electron irradiation to affect the electrical responses in diode performance. At 0.8 MeV, the forward and reverse currents of the irradiated nanodiodes deteriorated. Detailed information is summarized in Table 1. That is, the forward current decreased and the reverse

Table 1
Summarized Diode Performance before and after electron irradiation on p-Si/ZnO diode (Electrode radius: 80 μm and Al thickness: 100 nm).

Experimental condition	Reverse current at −3.0 V	Forward current at +3.0 V	Current ratio	V_{on}
No irradiation	−6.6E−8	2.5E−4	3.79E+3	2.3
0.8 MeV and 1000 kGy	−8.8E−7	1.2E−4	1.36E+2	2.1
0.8 MeV and 5000 kGy	−1.3E−7	2.1E−4	1.62E+3	2.2
0.8 MeV and 10,000 kGy	−1.2E−6	0.2E−4	1.67E+1	1.9
2.5 MeV and 1000 kGy	−1.2E−6	2E−5	1.67E+1	1.9
2.5 MeV and 5000 kGy	−8E−10	5.03E−5	6.29E+4	1.7
2.5 MeV and 10,000 kGy	−1.9E−9	4.5E−4	2.37E+5	1.5

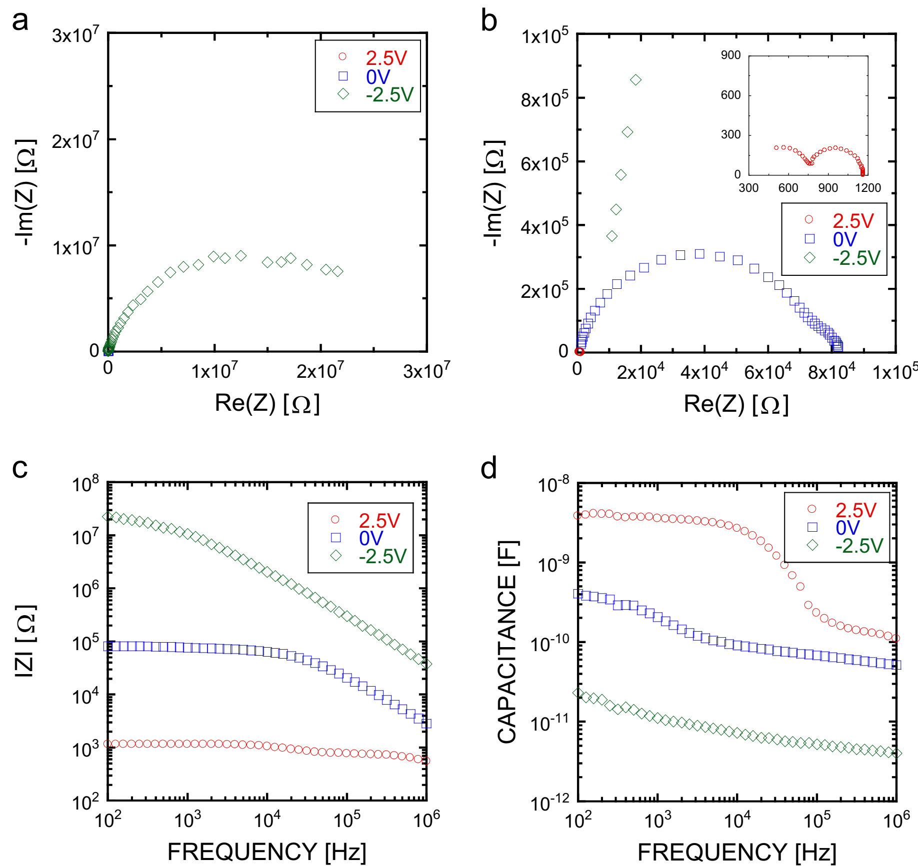

Fig. 4. Impedance spectra as a function of bias voltages obtained from p-Si/ZnO diodes (a) before electron beam irradiation. (b) shows an enlarged view of Fig. 4(a) (The inset shows an enlarged view of Fig. 4(a) at near the origin.) (c) and (d) describe bias-dependent absolute impedance and capacitance Bode plots, respectively, obtained as a function of applied bias voltages from p-Si/ZnO diodes.

current increased in comparison to the unirradiated ZnO-based nanodiodes. These current changes led to a lower current ratio. However, the high energy at 2.5 MeV induced significant changes not observed after irradiation at 0.8 MeV. As shown in Fig. 3(b), a low electron dose of 1000 kGy affected the ZnO-based nanodiodes in a manner similar to that at 0.8 MeV. Beginning with 5000 kGy, the electrical performance enhanced as the forward bias current increased and the reverse bias current decreased. These changes resulted in a high current ratio—60 times higher than that obtained in the case of nanodiodes unirradiated by an electron beam. After electron irradiation, the reverse current exhibited noticeable changes in magnitude. However, the ON-voltage for the forward current exhibited a small change in magnitude from 2.3 V to 1.5 V. Especially, the electron irradiation of 10,000 kGy at 2.5 MeV induced highly significant change in both forward and reverse currents, leading to the highest current ratio of 2.37×10^5.

Impedance spectroscopy was employed to understand the underlying mechanism in addition to the supplementary characterizations compared to the dc-based current–voltage characteristics (See Figs. 4 and 5). Figs. 4 and 5 show bias-dependent behaviors of resistance and impedance along with the effect of electron irradiation. First, the real-axis intercept of the real impedance part is denoted by the overall resistance provided by the nanodiodes. As shown in Figs. 4 and 5, the bias-dependent responses exhibit current–voltage characteristics and the resistance increases with increasing reverse voltage in the negative direction. However, as the bias voltage is changed to positive, the corresponding resistance decreases significantly, supporting the high conduction features found in the dc-based current–voltage characteristics of Fig. 3.

Impedance information can be transformed to the dielectric parameters through a conversion factor. The relationship between the impedance and capacitance is defined through the following equation involving complex variables

$$\mathrm{Re}(C) = \mathrm{Re}\left(\frac{1}{2\pi f Z}\right) = \frac{-\mathrm{Im}(Z)}{2\pi f[(\mathrm{Re}(Z))^2 + (\mathrm{Im}(Z))^2]} \quad (3)$$

where C and Z are the complex capacitance and impedance (whose components are real and imaginary ones), f is the frequency in Hz. Only the real capacitance, Re(C), is employed in order to describe the charging capability, or equivalently dielectric constants. As found in impedance-based responses, the capacitance also shows a bias-dependent behavior. For example, at 1 MHz, the capacitance increases with increasing applied bias from negative to positive bias. The increase in capacitance is attributed to the presence of depletion regions between p-type Si and n-type ZnO materials, corroborated by an extremely high dielectric constant of approximately 10,000. The effective dielectric constant is attributed to the shallow

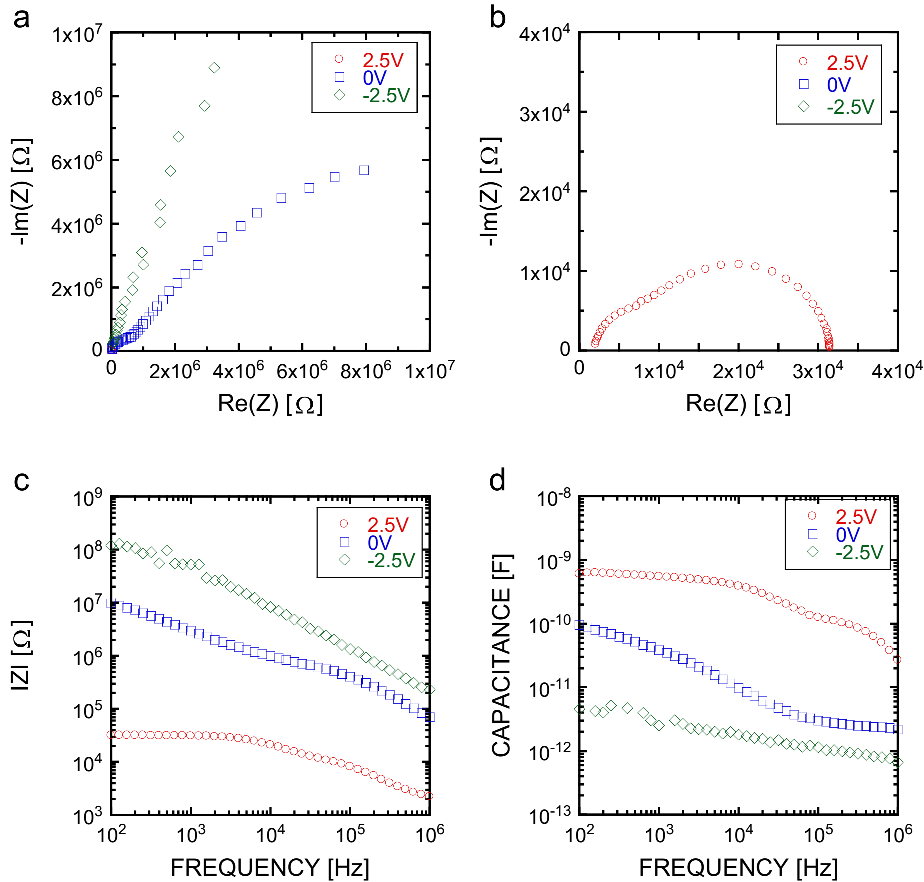

Fig. 5. Impedance spectra as a function of bias voltages obtained from p-Si/ZnO diodes (a) after electron beam irradiation at 2.5 MeV, (b) shows enlarged view of Fig. 5(a). (c) and (d) describe bias-dependent absolute impedance and capacitance Bode plots, respectively, obtained as a function of applied bias voltages from p-Si/ZnO nano-diodes.

thickness of the depletion region (approximately 30 nm) [14]. Moreover, the continuous change in capacitance at 1 MHz is believed to be associated with the dynamic change in volume that is responsible for charge storage as capacitors. As a result, the depletion region becomes narrower with increasing applied bias in the positive direction. Depending on the magnitude of applied voltage, the shape of the impedance spectra shows significant changes when analyzed by the unique equivalent circuits in which the resistors and/or capacitors (or constant-phase elements) are connected in series or in parallel [15]. At −2.5 V, the impedance becomes extremely large, showing only a partial portion of a single arc described by $R_0(R_1C_1)$ where R_0 is connected in series with a parallel connection of R_1 and C_1. However, at higher voltages (equal to or greater than 0 V), the impedance spectra is best modeled as $R_0(R_1C_1)(R_2C_2)$. The equivalent circuits are shown in Fig. 6. The analyzed circuit parameters are summarized in Table 2. In particular, the electron beam irradiation is believed to decrease the high-frequency capacitance, compared to that before irradiation. The presence of two RC circuits indicates that two different origins contribute to the effective impedance spectra. This implies that two different regimes are dependent on the applied bias. In the case of reverse bias, the impedance is determined by a single depletion. However, at higher voltages, the impedance spectra is controlled by either two depletion regimes of different time constants or a relative higher contribution of the electrode-related responses added to that of the depletion region.

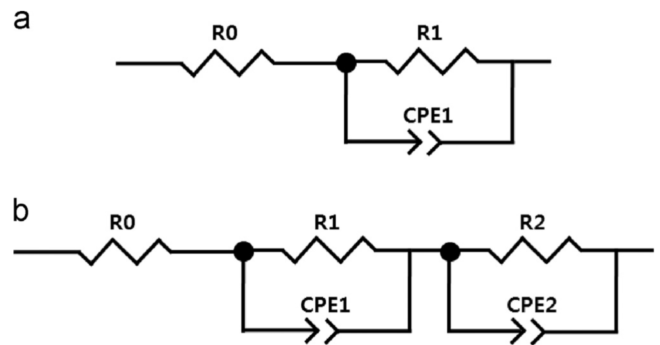

Fig. 6. Equivalent circuit models employed for impedance analysis of Figs. 4 and 5. (a) equivalent circuit model at negative bias and (b) equivalent circuit model at no and positive bias.

Noticeably, electron irradiation induces a reduction in the thickness of the depletion region. These phenomena are believed to be associated with electron injection into the junction regimes, affecting the additional change in transport from Si to ZnO or

Table 2
Analyzed equivalent circuit parameters from impedance spectra of Figs. 4 and 5.

	R_0	R_1	CPE_1	R_2	CPE_2
No irradiation at 0 V	618	7.0613E+04	2.6850E−10	1.1274E+04	5.8797E−08
No irradiation at +2.5 V	385.8	359.5	1.7730E−10	416.6	3.2823E−08
No irradiation at −2.5 V	–	2.5588E+07	5.1020E−11	–	–
2.5 MeV and 10,000 kGy at 0 V	–	4.9728E+05	1.4320E−11	2.0211E+07	8.9060E−10
2.5 MeV and 10,000 kGy at +2.5 V	2103	5914	1.5600E−10	2.3561E+04	2.0330E−09
2.5 MeV and 10,000 kGy at −2.5 V	–	1.9040E+08	1.6040E−11	–	–

from ZnO to Si. The interaction of the electron beam results in a reduction in the geometrical thickness in the depletion regions between p-Si and ZnO. This effect is reflected in the impedance spectra and capacitance Bode plots (Figs. 4 and 5). This can be explained using the energy band diagram proposed previously. The electron injection increases the thickness of the depletion region because of electronic concentration adjacent to or at the depletion zone between p-Si and ZnO. Moreover, the additional contribution of the injected electrons seems to increase the potential barrier compared to that observed in the case of un-irradiated p-n diodes.

In summary, electron irradiation influences nanodiodes comprising p-type Si and n-type ZnO. At lower acceleration voltages, the electron beam degrades the current–voltage characteristics. However, a higher acceleration voltage induces improvement in the diode performance, i.e., reduction in the reverse current and increase in the forward current. The improvement in nanodiode performance is attributed to the presence of bias-dependent depletion regions formed between heterogeneous semiconductors.

4. Conclusions

ZnO-based nanodiodes were fabricated through the atomic layer deposition of ZnO thin films onto p-type Si wafers. The current–voltage characteristics showed rectifying responses, depending on the polarity of the applied bias. Electron irradiation improved diode-based performance, i.e., reduction in the reverse current and increase in the forward current without significantly changing ON-voltages. This effect was probed using frequency-dependent impedance spectra, which demonstrated that the bias-dependent impedance and capacitance are attributed to the depletion regions formed between heterogeneous semiconductors and the modification of the energy band diagram due to electron injection in the depletion regions.

Acknowledgments

This research was supported by the Converging Research Center Program through the Ministry of Science, ICT and Future Planning, Korea (2013K000155), the Basic Science Research Program through the National Research Foundation of Korea (NRF) funded by the Ministry of Education, Science and Technology (2010-0009179), by the Nuclear Research & Development Program through the National Research Foundation of Korea(NRF) grant funded by the Ministry of Education, Science and Technology(MEST) (2011-0018915), and by the KIST research program (Grant 2E24001).

References

[1] C. Periasamy, P. Chakrabarti, Large-area and nanoscale n-ZnO/p-Si heterojunction photodetectors, Journal of Vacuum Science and Technology B 29 (2011) (051206-051206-6).

[2] I.S. Jeong, J.H. Kim, S. Im, Ultraviolet-enhanced photodiode employing n-ZnO/p-Si structure, Applied Physics Letters 83 (2003) 2946–2948.

[3] M. Izaki1, T. Shinagawa, K.-T. Mizuno, Y. Ida, M. Inaba, A. Tasaka, Electrochemically constructed p-Cu_2O/n-ZnO heterojunction diode for photovoltaic device, Journal of Physics D: Applied Physics 40 (2007) 3326–3329.

[4] E. Nannen, T. Kümmell, A. Ebbers, G. Bacher, p-Si/n-ZnO Nanocrystal heterojunction light emitting device, Applied Physics Express 5 (2012) (035001-035001-3).

[5] B.S. Kang, S.-E. Ahn, M.-J. Lee, G. Stefanovich, K.H. Kim, W.X. Xianyu, C.B. Lee, Y. Park, I.G. Baek, B.H. Park, High-current-density CuO_x/$InZnO_x$ thin-film diodes for cross-point memory applications, Advanced Materials 20 (2008) 3066–3069.

[6] S. Mridha, D. Basak, Aluminium doped ZnO films: electrical, optical and photoresponse studies, Journal of Physics D: Applied Physics 40 (2007) 6902–6907.

[7] R. Tongpool, C. Leach, R. Freer, Temperature and microstructural dependence of the sensitivity of heterocontacts between zinc oxide and copper oxide in reducing environments, Journal of Materials Science Letters 19 (2000) 119–121.

[8] G. Rius, I. Martín, P. Godignon, A. Bachtold, J. Bausells, E. Lora-Tamayo, F. Pérez-Murano, Response of carbon nanotube transistors to electron beam exposure, Microelectronic Engineering 84 (2007) 1596–1600.

[9] D.W. Ranasinghe, D.J. Machin, G. Proctor, Electron beam irradiation effects on MOS-transistors and its significance to E-beam testing, Microelectronic Engineering 7 (1987) 397–403.

[10] I. Childres, L.A. Jauregui, M. Foxe, J. Tian, R. Jalilian, I. Jovanovic, Y.P. Chen, Effect of electron-beam irradiation on graphene field effect devices, Applied Physics Letters 97 (2010) (173109-173109-3).

[11] X. Li, S.Q. Gu, E.E. Reuter, J.T. Verdeyen, S.G. Bishop, J.J. Coleman, Effect of e-beam irradiation on a p-n junction GaN light emitting diode, Applied Physics Letters 80 (1996) 2687–2690 (80[5]).

[12] C.-R. Park, H.-K. Lee, J.-H. Hwang, Y.-H. Hahn, B.-C. Lee, K.-S. An, Nonvolatile memory characteristics induced in high-k dielectric thin films through electron irradiation, Journal of the Korean Physical Society 59 (2011) 726–729.

[13] H. Fujiwara, Spectroscopic Ellipsometry: Principles and Applications, first ed., John Wiley & Sons, Ltd., West Sussex, England, 2007.

[14] J.T.S. Irvine, D.C. Sinclair, A.R. West, Electroceramics: characterization by impedance spectroscopy, Advanced Materials 2 (1990) 132–138.

[15] E. Barsoukov, J.R. Macdonald, Impedance Spectroscopy: Theory, Experiment, and Applications, second ed., John Wiley & Sons, Inc., New York, 2005.